Finite-Volume Calculation of Inviscid Transonic Airfoil-Vortex Interaction

Murali Damodaran* and David A. Caughey†
Cornell University, Ithaca, New York

Unsteady inviscid transonic airfoil-vortex interaction is numerically analyzed by solving the two-dimensional unsteady Euler equations in integral form using a finite-volume scheme. The solution procedure is based on an explicit Runge-Kutta time-stepping scheme wherein the spatial terms are central-differenced and a combination of second- and fourth-differences in the flow variables is used to form the numerical dissipation terms to stabilize the scheme. A velocity decomposition technique is applied to alleviate the problem of vortex diffusion by the numerical dissipation terms and to treat the interaction of a Rankine vortex with an airfoil accurately. Results obtained are compared with available numerical data.

I. Introduction

An unsteady flow feature of helicopter rotor blades in forward flight can be caused by interaction with the trailing tip vortex of a preceding blade and hence blade-vortex interactions often occur. The interaction of the trailing tip vortex wake with oncoming rotor blades can induce unsteady aerodynamic blade loading resulting in aeroelastic instabilities, blade vibrations, and also in the generation of a highly directional impulsive noise. In view of the use of large aspect ratio blades in modern military combat helicopters, the flow near the tip of the rotor blade is transonic, highly nonlinear, and complex. The blades trail strong tip vortices that trace out helical paths in space, leading to a variety of possible blade-vortex interactions. Figure 1a shows one such interaction that is an unsteady, three-dimensional close encounter of a curved line vortex at an arbitrary intersection angle Λ with a large aspect ratio helicopter blade. Under certain flight conditions, a blade can encounter a vortex that is almost parallel to itself, i.e., $\Lambda = 0$. Such an encounter is essentially two-dimensional but unsteady, since the problem can approximately be modeled as the interaction of an infinitely long line vortex with an infinitely long blade parallel to the line vortex. The schematic of this particular blade-vortex interaction that is investigated in this work is shown in Fig. 1b.

In recent years, the airfoil-vortex interaction problem has received considerable attention in the helicopter industry, primarily motivated by the goal of designing an aerodynamically efficient and quiet blade. Until recently, this problem could be studied using only simple aerodynamic modeling such as conformal mapping procedures using incompressible thin-airfoil theory, e.g., Huang and Chow.[1] However, with rapid advances made in numerical techniques and the availability of fast computers, more elements in the problem of transonic airfoil-vortex interaction have become tractable in recent years.

The problem has been studied using the transonic small-disturbance theory by McCroskey and Goorjian[2] who solved this equation along with the small-disturbance boundary conditions using the time-accurate implicit numerical algorithm of Ballhaus and Goorjian.[3] In a separate work, Caradonna et al.[4] studied this problem using the same model by introducing a cut in the computational domain downstream of the passing vortex, across which the velocity potential was allowed to be discontinuous. More recently, George and Chang[5] extended the method by employing a vortex-in-cell method with multiple branch cuts to correct for the potential jumps due to the distributed vortices representing the vortex core.

The full-potential model removes some limitations of the small-disturbance approach. Such a model for the transonic airfoil-vortex interaction problem has been considered by Jones.[6] Such methods solve the full-potential equation without invoking any small-disturbance or low-frequency assumptions, but the representation of the airfoil geometry requires using a body-fitted coordinate system. Treating this problem using the potential equation requires fitting the vortex into the flowfield because the potential methods are based on the assumption of irrotationality and hence do not have any mechanism to represent rotational regions in the flowfield.

A more complete model for this problem can be based on the Euler or Navier-Stokes equations. Numerical solutions to these equations do not require fitting of vortices into the flowfield because the structure of these equations includes the proper physics to include vortical regions. The major limitation of the finite-difference solution of these equations for vortical flows is the diffusion of vorticity introduced by the numerical dissipation inherent in the schemes. This is a major drawback because a compact vortex introduced at the boundary of the computational domain will diffuse as it is convected past the airfoil, and hence the load variation due to the interaction will be incorrectly predicted. Steger and Kutler[7] suggested the use of higher-order differencing and grid refinement along the path of the vortex to alleviate this problem. This increases the computational effort and except where the vortex position is known a priori, some form of adaptive grid refinement procedure is required, which further increases the coding complexity. Srinivasan et al.[8-9] developed a procedure for solving this problem using the Euler and thin-layer Navier-Stokes equations. In their approach, the dependent flow variables are split into a prescribed part that defines the vortical disturbance and a remaining part that is obtained from the solution of the governing equations. Specifically, the dependent variables are decomposed into $q = q_v + (q - q_v)$, where q is the flow vector $[\rho,\rho u,\rho v,\rho E]^T$ and

Presented as Paper 87-1244 at the AIAA 19th Fluid Dynamics, Plasma Dynamics, and Lasers Conference, Honolulu, HI, June 8-10, 1987; received Aug. 26, 1987; revision received March 2, 1988.

*Currently National Research Council Research Associate, NASA Ames Research Center, Moffett Field, CA. Member AIAA.

†Professor, Sibley School of Mechanical and Aerospace Engineering. Associate Fellow AIAA.

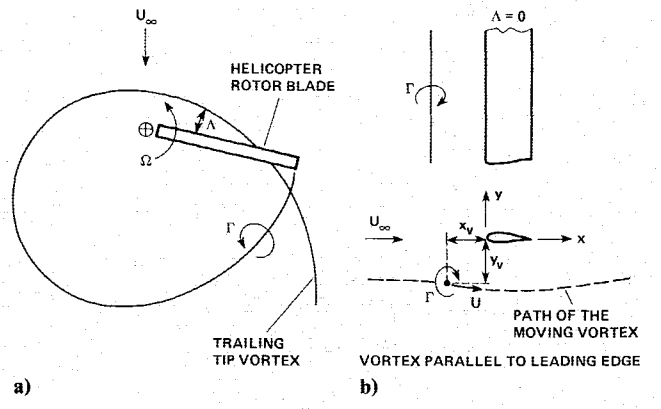

a) b)

Fig. 1 Schematic representation of helicopter blade-vortex interaction and the limiting case of a two-dimensional airfoil-vortex interaction under certain flight conditions.

q_v represents the flowfield associated with the vortical disturbance. The unsteady two-dimensional thin-layer Navier-Stokes equations, modified to implement the perturbation scheme of Buning and Steger[10] to resolve the incoming nonuniform stream due to the vortex without having to resort to any far-field grid refinement, are then solved numerically by an implicit finite-difference procedure. Sankar and Tang[11] and Wu et al.[12] solved this problem by employing an alternating direction implicit procedure to solve the Navier-Stokes and Euler equations along the lines of the implicit approximate factorization scheme of Beam and Warming[13] by modifying the numerical dissipative operator to act on the difference between the instantaneous total field values and the vortex field values, thereby minimizing vortex diffusion. More recently, Rai[14] simulated this problem by solving the thin-layer Navier-Stokes equations using a fifth-order accurate upwind-biased scheme on a multizone patched grid around the airfoil. The strength of this ambitious work lies in its ability to preserve the vortex structure over long periods of travel and to avoid using vortex preservation techniques, thereby rendering its ability to treat strong airfoil-vortex interactions.

In the present work, the unsteady Euler equations are solved on a body-fitted grid about an airfoil in two-dimensions to study unsteady inviscid interaction of a Rankine vortex with a stationary airfoil. The finite-volume scheme proposed by Jameson et al.[15] that solves the integral form of the unsteady Euler equations by an explicit multistage time-stepping numerical scheme is used to study this problem. Section II presents the details of the formulation of the present approach. Section III presents numerical results and discussion.

II. Formulation

A. Numerical Scheme

The unsteady Euler equations for two-dimensional inviscid flow can be written in integral form for a region A with a boundary B as

$$\frac{\partial}{\partial t}\int\int_A w\,dx\,dy + \int_B (f\,dy - g\,dx) = 0 \tag{1}$$

where

$$w = [\rho,\rho u,\rho v,\rho E]^T$$

$$f = [\rho u,\rho u^2 + p,\rho vu,\rho Hu]^T$$

$$g = [\rho v,\rho uw,\rho v^2 + p,\rho Hv]^T$$

Here, p, ρ, u, v, E, and H are the pressure, density, Cartesian velocity components, specific total energy, and specific total enthalpy. $H = E + (p/\rho)$ and for a perfect gas, $E = [p/(\gamma - 1)\rho] + (1/2)(u^2 + v^2)$. The pressure and density are scaled by the freestream values p_∞ and ρ_∞. The velocities are scaled by $a_\infty/\sqrt{\gamma}$, where a_∞ is the speed of sound and γ is the ratio of the specific heats of the gas. All lengths are scaled by the chord c of the airfoil.

In order to derive a semidiscrete model to treat arbitrary complex geometric domains, the physical domain is divided into quadrilateral cells labeled by the subscripts i,j. A system of ordinary-differential equations for the average values of the dependent variables is obtained by applying the integral law, Eq. (1), separately to each cell. These equations have the form

$$\frac{d}{dt}(hw)_{i,j} + Q_{i,j} = 0 \tag{2}$$

where $h_{i,j}$ is the area and $Q_{i,j}$ is the net flux out of the cell whose location in the physical space is denoted by the ith and the jth coordinates. This flux can be written as

$$Q_{i,j} = \sum_{k=1}^{k=4} (f\Delta y - g\Delta x) \tag{3}$$

where Δx and Δy are the increments in the x and y directions along the kth face of the cell. On a sufficiently smooth mesh, this approximation is second-order accurate. In order to maintain stability, to suppress the tendency for odd and even point oscillations, and to limit undesirable overshoots near discontinuities such as shock waves, Eq. (2) must be supplemented by dissipative terms. Equation (2) then becomes

$$\frac{d}{dt}(hw)_{i,j} + Q_{i,j} - D_{i,j} = 0 \tag{4}$$

where $D_{i,j}$ represents the dissipative terms that are constructed by blending second- and fourth-difference terms in flow variables as described in Jameson et al.[15] These equations are then advanced in time from a set of initial conditions using a four-stage Runge-Kutta time-stepping scheme that preserves a second-order temporal accuracy. The reader is encouraged to refer to Refs. 15–17 for specific details of the numerical scheme.

B. Vortex Model

For simulating the airfoil-vortex interaction problem, an appropriate representation of a practical vortex needs to be chosen. For the present study, a Rankine vortex with a finite core is chosen to interact with the airfoil. The principal parameters that characterize the vortex are its strength $\hat{\Gamma}$ and the radius of its core $\hat{r}_c$. The nondimensional vortex strength is $\Gamma = (\hat{\Gamma}\sqrt{\gamma}/a_\infty c)$ and the nondimensional vortex core radius is $r_c = (\hat{r}_c/c)$. The position of the vortex is denoted by the coordinates x_V, y_V. For a given vortex strength, using Kutta-Joukowski theorem, it is possible to identify an equivalent lift coefficient C_{LV}:

$$C_{LV} = (2\Gamma/M_\infty\sqrt{\gamma}) \tag{5}$$

The cylindrical velocity distribution q_V corresponding to the Rankine vortex at a point at a distance r from the vortex core center is given by

$$q_V = (\Gamma/2\pi r) \qquad \text{for } r > r_c \tag{6a}$$

$$q_V = (\Gamma r/2\pi r_c^2) \qquad \text{for } 0 < r < r_c \tag{6b}$$

The vortex core is a rotational region and contains all the vorticity associated with the vortex.

The pressure field induced by the vortex in a uniform freestream can be determined using the radial momentum equation:

$$\frac{dp_V}{dr} = \frac{\rho_V q_V^2}{r} \tag{7}$$

where p_V is the pressure field induced by the vortex, and ρ_V is the density field induced by the vortex. For transonic flows, since the density is not constant, the pressure field is determined using Eq. (7) in conjunction with the constant enthalpy flow relation:

$$(\gamma/\gamma - 1)(p_V/\rho_V) + (q_V^2/2) = (\gamma/\gamma - 1)(p_\infty/\rho_\infty) \tag{8}$$

From Eq. (8), an expression for the density ρ_V can be obtained, and this expression is introduced in place of ρ_V in Eq. (7). For the velocity distribution corresponding to a Rankine vortex, it is possible to integrate Eq. (7) analytically to obtain the pressure distribution outside and inside the vortex core. The constants of this integration are evaluated by assuming that far away from the vortex, the pressure attains the freestream value and by matching the pressures at the edge of the vortex core, i.e., $r = r_c$.

In order to treat the transonic airfoil-vortex problem, the steady-state transonic flow past an airfoil is first determined. The vortex is then introduced into the transonic flowfield at a point upstream of the airfoil. When the vortex structure is specified as an initial condition, the numerical scheme captures the vortex in the sense that no explicit tracking of the vortex is required in its subsequent convection. The initial conditions simulating the vortex can be constructed by superposing the vortex flowfield perturbations upon the steady transonic flow variables at all the points in the physical domain. The perturbations that result when the vortex is introduced in a uniform compressible flowfield can be computed as follows:

$$\Delta\rho = \rho_V - \rho_\infty, \qquad \Delta p = p_V - p_\infty$$
$$\Delta u = u_V, \qquad \Delta v = v_V \tag{9}$$

where u_V and v_V are the Cartesian components of the velocity distribution q_V corresponding to the vortex. The initial conditions simulating the presence of an isolated vortex in a transonic flowfield can be constructed as follows:

$$\rho = \rho_S + \Delta\rho, \qquad p = p_S + \Delta p$$
$$u = u_S + \Delta u, \qquad v = v_S + \Delta v \tag{10}$$

where p_S, ρ_S, u_S, and v_S are the pressure, density, and velocity-field components respectively associated with the steady transonic flow around the airfoil.

Time-accurate calculations are started from this initial guess, integrating Eq. (1) on a fixed grid to predict how the initial vortical disturbance convects through the computational grid. However, the numerical dissipation associated with the finite grid spacing progressively weakens the gradients in the vortex and diffuses it, thereby reducing its strength. This results in an inaccurate prediction of the load variation on the airfoil as the vortex convects past it. This problem is severe in regions where the mesh is coarse. Near the airfoil where the mesh is dense, this is not a problem.

C. Velocity Decomposition

In order to prevent the vortex from being diffused, the governing Euler equations are modified by introducing a velocity-field decomposition. The basis of this approach is to decompose the total velocity field into two parts, the first part being the induced velocity field of the vortex and the second part being the difference between the total velocity and the vortex-induced velocity, here called the velocity perturbation. This second part is unknown and is determined in the course of the computation. If q is the total velocity, q_V is the vortex-induced velocity, and u_p and v_p are components of the unknown perturbation velocity q_p; then it is possible to write the following relation for the total velocity field:

$$q = q_V + (q - q_V) = q_V + q_p \tag{11}$$

where $q_p = q - q_V$ is the unknown perturbation quantity that will be computed.

Introducing the velocity-field decomposition into the integral form of the unsteady Euler equations, Eq. (1), gives

$$\frac{\partial}{\partial t}\int\int_A w_p \, dx \, dy + \int_B (f_p \, dy - g_p \, dx) + S = 0 \tag{12}$$

where

$$w_p = [\rho, \rho u_p, \rho v_p, \rho E]^T$$

$$f_p = \begin{bmatrix} \rho(u_p + u_V) \\ \rho u_p(u_p + u_V) + p \\ \rho v_p(u_p + u_V) \\ \rho H(u_p + u_V) \end{bmatrix}, \qquad g_p = \begin{bmatrix} \rho(v_p + v_V) \\ \rho u_p(v_p + v_V) \\ \rho v_p(v_p + v_V) + p \\ \rho H(v_p + v_V) \end{bmatrix}$$

$$S = \begin{bmatrix} 0 \\ \dfrac{\partial}{\partial t}\displaystyle\int\int_A \rho u_V \, dx \, dy + \int_B \rho u_V(u_p + u_V) \, dy - \rho u_V(v_p + v_V) \, dx \\ \dfrac{\partial}{\partial t}\displaystyle\int\int_A \rho v_V \, dx \, dy + \int_B \rho v_V(u_p + u_V) \, dy - \rho v_V(v_p + v_V) \, dx \\ 0 \end{bmatrix}$$

The components of the vortex-induced velocity, i.e., u_V and v_V satisfy the following relations along the path traced out by the vortex during its convection:

$$\frac{\partial u_V}{\partial t} = -u_c \frac{\partial u_V}{\partial x} - v_c \frac{\partial u_V}{\partial y} \tag{13a}$$

$$\frac{\partial v_V}{\partial t} = -u_c \frac{\partial u_V}{\partial x} - v_c \frac{\partial v_V}{\partial y} \tag{13b}$$

where u_c and v_c are the vortex convection velocities. The flux terms contained in S in Eq. (12) can be evaluated using Eq. (13) and Eq. (6).

A quasisteady airfoil-vortex interaction resulting from a stationary isolated vortex in the vicinity of the airfoil can be computed by setting $u_c = 0$ and $v_c = 0$ and using some of the convergence acceleration schemes described in Refs. 15–17. In this study, local time stepping has been used to calculate the quasisteady interaction. Forced airfoil-vortex interaction that results when the vortex is constrained to move at the freestream velocity can be simulated by setting the convection velocity components u_c and v_c to the freestream velocity components. Free airfoil-vortex interaction that results when the vortex convects at the local fluid velocity can be simulated by tracking the vortex in Langrangian coordinates, i.e.,

$$\frac{dx}{dt} = u_c, \qquad \frac{dy}{dt} = v_c \tag{14}$$

These equations are integrated explicitly to give the path of the vortex. After each time step, a search is made for the grid points surrounding the vortex, and a bilinear interpolation scheme is used to estimate the local convection velocities u_c and v_c from the velocities at these grid points. Forced and free interactions are unsteady and hence time-accurate computations are performed to obtain the evolution of the unsteadi-

ness. The initial conditions for starting the time-accurate calculation of the moving vortex-airfoil interaction cases are obtained by computing the quasisteady vortex-airfoil interaction when the vortex is placed at its initial position upstream of the airfoil.

The decomposition splits the velocity field into a part containing the vorticity associated with the isolated vortex and a part that contains the vorticity shed from the trailing edge and that generated by the shocks near the airfoil surface. The perturbation velocity field u_p is smooth while the vortex-induced velocity varies rapidly in the vicinity of the vortex core. An advantage of this decomposition is that the numerical dissipation terms in the momentum equations need be applied only to the perturbation component of the momentum, i.e., ρq_p, rather than the total momentum. Thus, the numerical dissipation does not act on the vortex, and hence the vorticity associated with the vortex will not be diffused. This formulation circumvents the need for high resolution in regions of large flow gradients near the vortex core.

D. Grid and Boundary Conditions

All calculations reported here are performed on a stretched C-grid generated by a sheared parabolic transformation. The boundary conditions are applied to the total flowfield variables. The far-field boundary conditions are based on the Riemann invariants approach as outlined in Refs. 15–17. On the airfoil surface, the normal total velocity component is set to zero, pressure is extrapolated from the interior, and density computed such that the normal entropy (p/ρ^γ) gradient is zero so as to minimize false entropy production. The values of vortex-induced velocities in the dummy cells erected outside the physical domain of interest are simply extrapolated from the corresponding values in the interior cells closest to these boundaries. The inflow boundary is located at about 80 chords from the airfoil leading edge while the outflow boundaries are located at about 20 chords from the airfoil trailing edge. Further details of the numerical calculation of the transonic airfoil-vortex interaction problem are given in Damodaran.[18]

III. Results and Discussion

For the purpose of comparing current results with available numerical data, all the calculations reported below use a Rankine vortex of strength 0.1893 (equivalent lift coefficient of 0.4), a core radius of 5% of the airfoil chord and having a clockwise sense interacting with a stationary NACA 0012 airfoil in transonic flow (left to right) at Mach number $M_\infty = 0.8$ and angle of attack $\alpha = 0$ deg. The initial location of the vortex is at a point 5.0 chords upstream of the airfoil leading edge and 0.26 chords below. Calculation is continued until the vortex has reached a point about 4.0 chords aft of the leading edge. The calculation was performed on a C-grid having 192 cells in the wrap-around direction and 32 cells in the normal direction. The computation was carried out on an IBM 3090/400 system and required a CPU time of 1.36×10^{-4} s per grid node per time step. The numerical scheme required about 5380 time steps to move the vortex a total of 9.2 chord lengths.

A. Rationale for Decomposition Form

In order to provide the rationale for integrating the decomposed form of the Euler equations for the airfoil-vortex interaction problem, a solution is obtained without the use of velocity decomposition. The intitial conditions are constructed using Eqs. (10), and Eq. (1) is integrated numerically. Figure 2a shows the variation of the aerodynamic force and quarter-chord pitching moment coefficients with the instantaneous vortex position that is assumed to move at the freestream velocity. The resulting interaction can be seen to be weak and the load variation on the airfoil is grossly underpredicted when compared with Fig. 3. Figure 2b shows the variation of

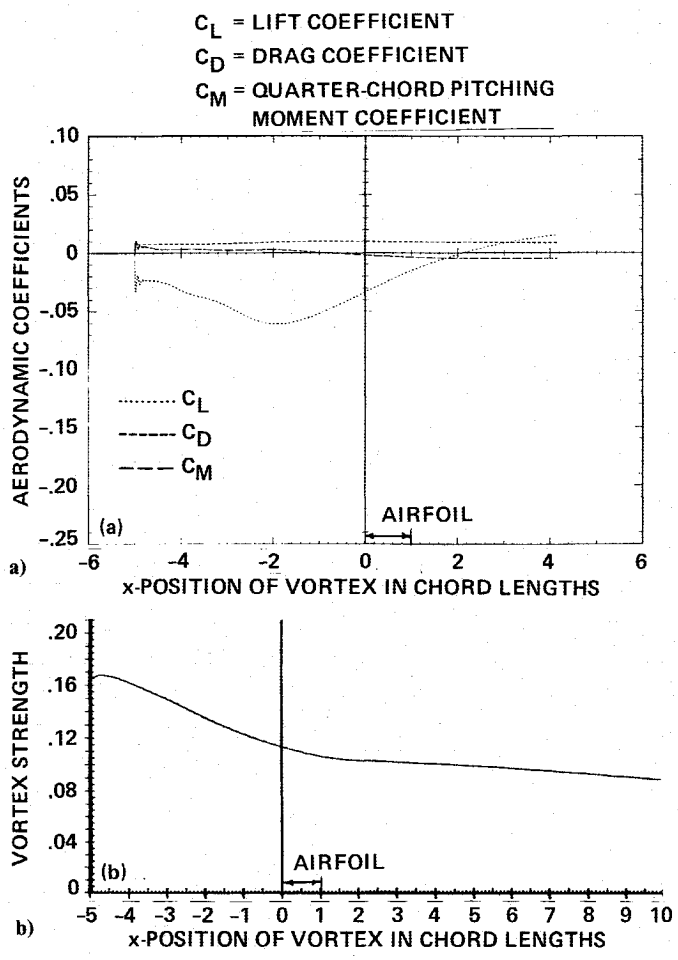

Fig. 2 Variation of a) aerodynamic coefficients, and b) vortex strength with instantaneous x position of the vortex using the undecomposed Euler equations.

the strength of the vortex that is estimated by evaluating the line integral of the total velocity field along a path traversing the limits of the physical domain but excluding the airfoil, the details of which can be found in Damodaran.[18] The vortex strength can be seen to be rapidly decreasing upstream of the airfoil while the rate of decrease slows down in the vicinity of the airfoil. The rapid decrease upstream of the airfoil is due to the greater numerical dissipation resulting from the coarseness of the grid in the far field. Near the airfoil the grid is finer and hence the amount of numerical dissipation is reduced. In both regions, however, the numerical dissipation acts on the total flowfield and progressively weakens all large gradients in the vicinity of the vortex core, so that by the time the vortex reaches the vicinity of the airfoil, the vortex is highly diffused, resulting in a weak interaction. This clearly demonstrates the drawback of using the undecomposed form of the Euler equations. This inaccuracy is efficiently dealt with by studying the airfoil-vortex interaction problem using the decomposed form of the Euler equations, Eq. (12), as demonstrated in the following calculations.

B. Unsteady Forced Interaction

The calculation of quasisteady airfoil-vortex interaction is started from the steady-state solution of transonic flow past the airfoil at Mach number 0.8 and angle of attack of 0 deg as the initial condition. The vortex velocity fields are then introduced into the flux terms of Eq. (12). The calculation is continued until the transients caused by introducing the vortex disappear and the flowfield becomes invariant with the

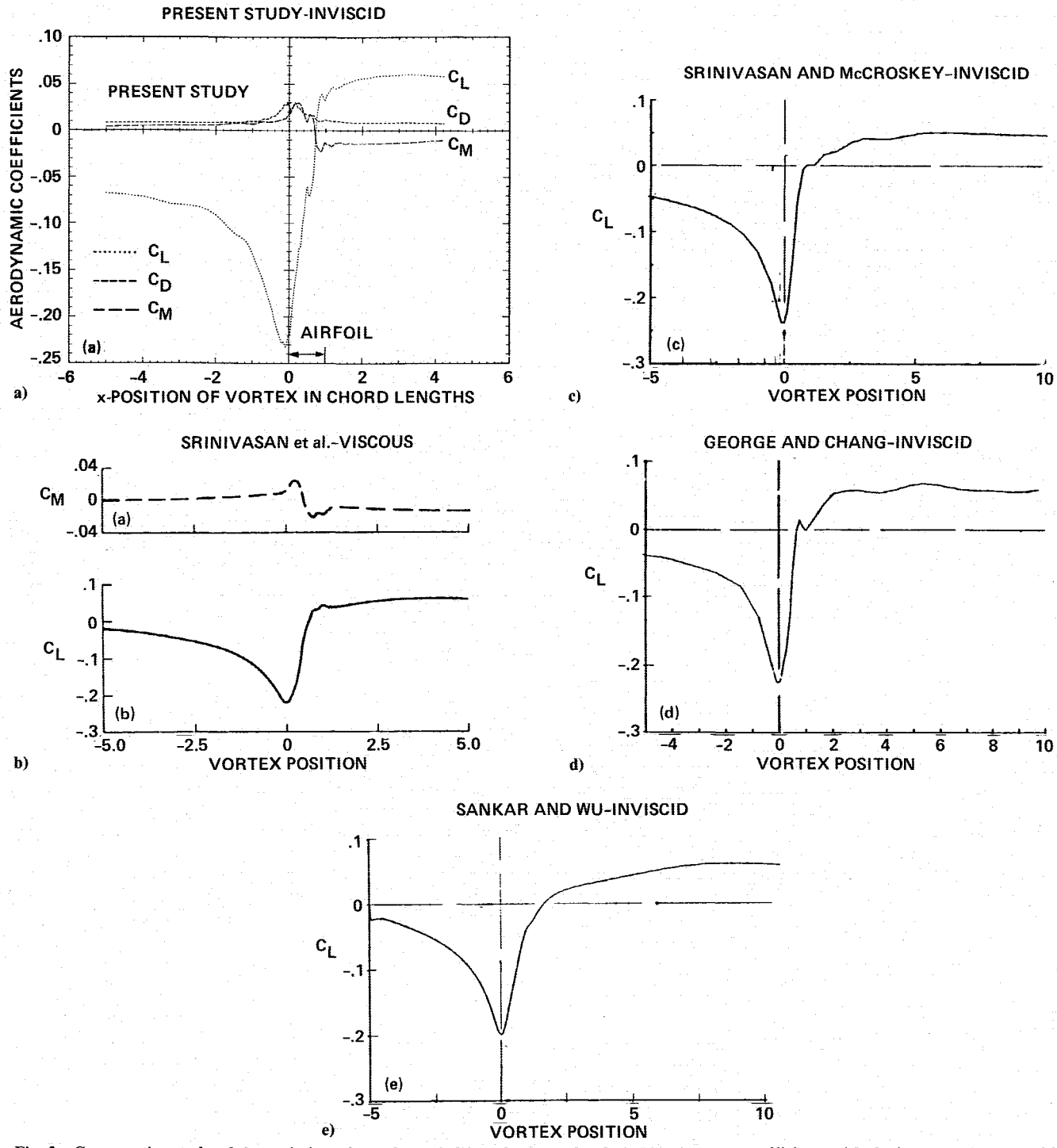

Fig. 3 Comparative study of the variation of aerodynamic lift and quarterchord pitching moment coefficients with the instantaneous x position of the vortex during forced airfoil-vortex interaction: a) present study, and b–e) others.

number of local time steps. Details are given in Damodaran.[18]

Using the quasisteady solution as an initial condition, the interaction resulting from the vortex constrained to convect with the freestream velocity is computed next. This is a good approximation when the vortex does not pass too near the airfoil. Figure 3a shows the variation of aerodynamic force and quarter-chord pitching moment coefficients with the instantaneous x position of the vortex. Since the vortex has a clockwise sense, when the vortex is ahead of the airfoil, it induces spatially varying velocities that result in negative angles of attack at the airfoil. This influence changes to increasing angles of attack as soon as the vortex has convected past the leading edge of the airfoil. The result obtained by the present study is shown in Fig. 3a. Figure 3b shows the corresponding viscous results of Srinivasan et al.[9] The corresponding inviscid results of other investigators from Ref. 19 are shown in Figs. 3c–3e, respectively. The variation of the lift coefficient is qualitatively the same as that obtained by other investigations. Severe load variations occur when the vortex is a few chords upstream of the airfoil. It should be noted that the initial lift on the airfoil without the vortex in the flowfield is zero (nonlifting case) and that any lift generated during the interaction is induced by the vortex. The maximum influence of the vortex on the airfoil flowfield seems to occur when the vortex is within 1 chord length of the airfoil. The minimum lift coefficient that occurs when the vortex reaches the leading edge has a value of about -0.24, which is in good agreement with other predictions shown in Fig. 3.

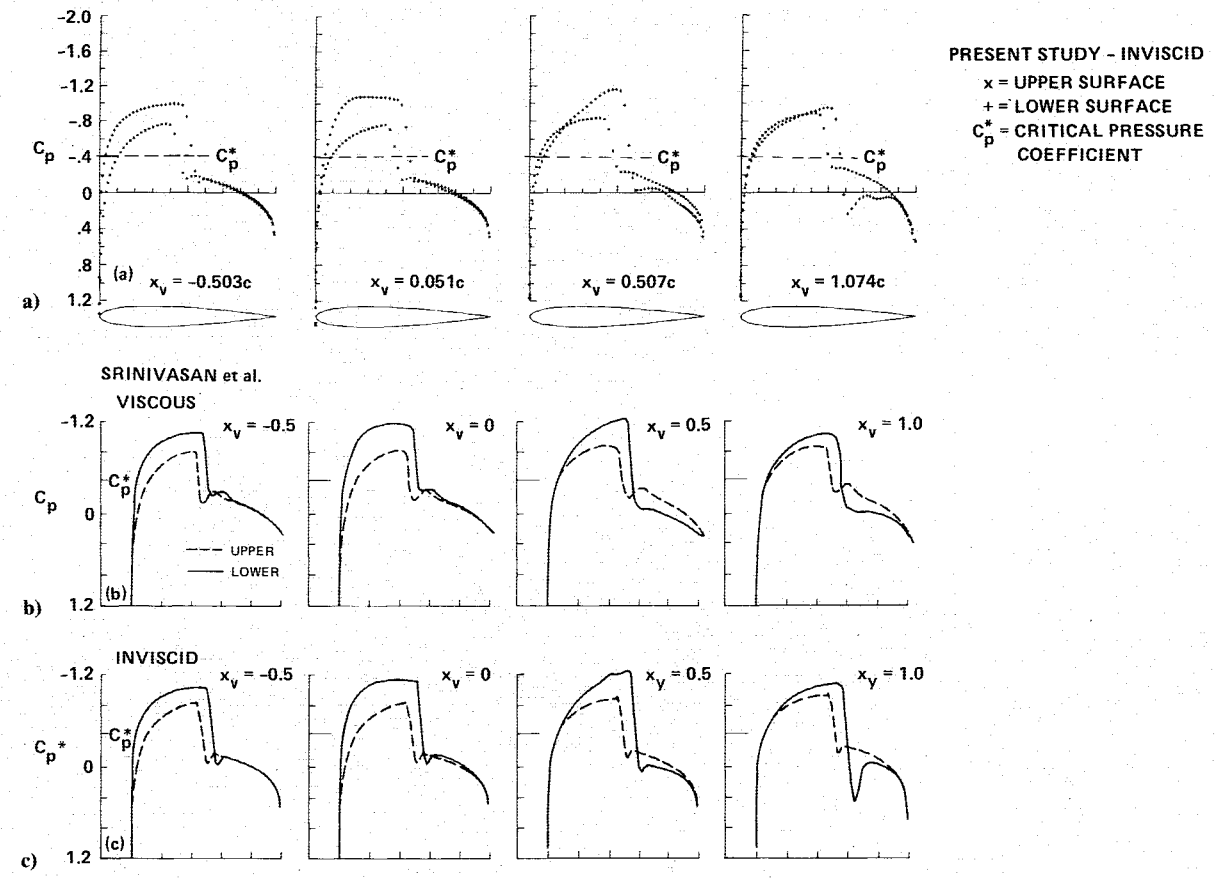

Fig. 4 Comparative study of the variation of the airfoil surface pressure distribution during forced airfoil-vortex interaction: a) present study, b), and c) Refs. 9 and 20.

The airfoil surface pressure distributions at selected instantaneous positions of the vortex between the leading edge and the trailing edge, obtained by the present calculation, are shown in Fig. 4a. The corresponding pressure distributions (viscous and inviscid) computed by Srinivasan et al.[9] and Srinivasan[20] also shown in Figs. 4b–4c, respectively, compare favorably with the current results. The resulting shock motions are evident from this figure. Figure 5 shows the contours of Mach number, pressure coefficient, and vorticity and the variation of the size of the supersonic regions. These plots help in visualizing the unsteady interaction. As the vortex passes below the airfoil, it encounters the shock on the lower surface of the airfoil. From Fig. 5, it can be seen that the vortex has split the lower shock wave in the flowfield into a triple shock wave. This is consistent with similar observations reported in Srinivasan et al.[9] The close agreement of viscous and inviscid results reported in Srinivasan et al.[8] suggests the adequacy of the inviscid model for this problem as long as strong interactions resulting in separated flow do not occur.

Another interesting aspect of this calculation, as demonstrated in Fig. 5, is the ability of the numerical scheme to preserve the vortex structure and prevent it from diffusing and losing its strength caused by the action of the numerical dissipation terms. The vorticity contours in Fig. 5 show how the vortical region undergoes shape distortions as the vortex passes below the airfoil. As the vortex passes below the airfoil, it enters the supersonic region and subsequently interacts with the shock. Vorticity is produced at the shock fronts, and the shape of the vortical region associated with the vortex distorts as a result of interacting with the vorticity produced at the shock. It must also be noted that although q_P is relatively smooth, there are small but abrupt changes in this quantity in the vicinity of the vortex core that are produced primarily by the flux terms of Eq. (12) that contains the instantaneous vortex velocity fields. However, these changes in q_P are quite small compared to the values of q_V in the vicinity of the vortex core. The numerical dissipation operates on q_P, and the presence of these small peaks in the vicinity of the core will result in a slight spreading of this quantity. This also contributes to the shape distortions of the vortical region as it convects past the airfoil. The rapidly changing lift coefficient causes wake vorticity to be shed from the airfoil trailing edge as shown in the vorticity contours in Fig. 5. Since the vortex is very close to the airfoil, some kind of merging with the wake vorticity appears to be taking place after the vortex has traveled through the supersonic pockets and past the trailing edge.

C. Unsteady vs Quasisteady Interactions

The difference between quasisteady airfoil-vortex interaction and moving airfoil-vortex interaction is assessed next. Figure 4b shows the airfoil surface pressure distribution corresponding to the moving vortex case when the vortex has reached a point that is 0.051 chord lengths aft of the leading edge and -0.26 chord lengths below the airfoil. The quasisteady interaction corresponding to a fixed vortex at this position is calculated, and the corresponding quasisteady airfoil surface pressure distribution is shown in Fig. 6. The lift and drag coefficients for the unsteady interaction at this vortex location are $C_L = -0.208$ and $C_D = 0.0225$, whereas those for the quasisteady interaction are $C_L = -0.4520$ and $C_D = 0.0435$. The aerodynamic force coefficients for the quasisteady interaction are significantly higher than the values corresponding to the unsteady interaction. The airfoil surface pressure distributions for the two cases are significantly different and so are the contours of Mach number and pressure coefficient, as can be seen by comparing Figs. 4a and 5 with Fig. 6. For the quasisteady interaction at this location, the

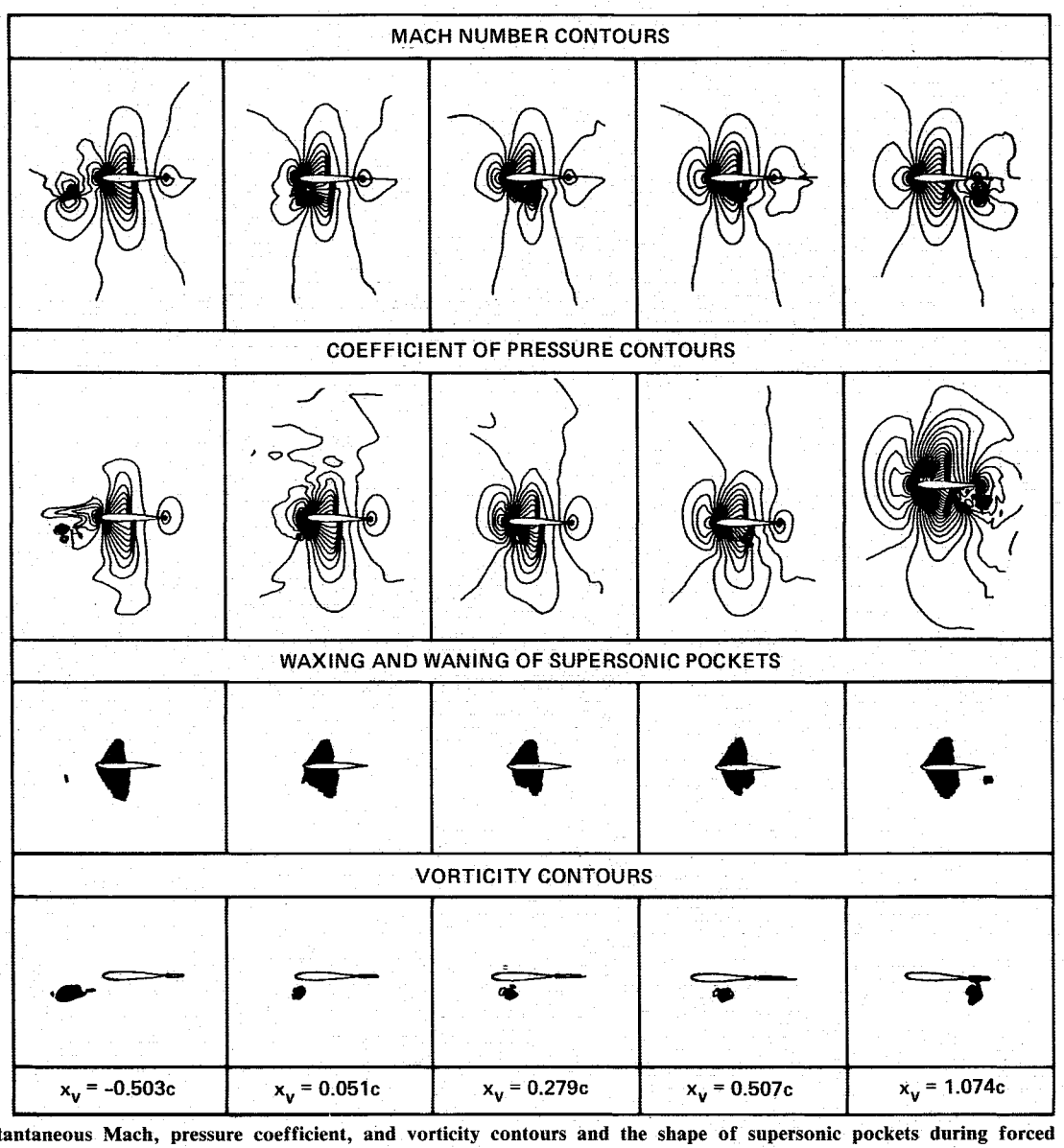

Fig. 5 Instantaneous Mach, pressure coefficient, and vorticity contours and the shape of supersonic pockets during forced airfoil-vortex interaction.

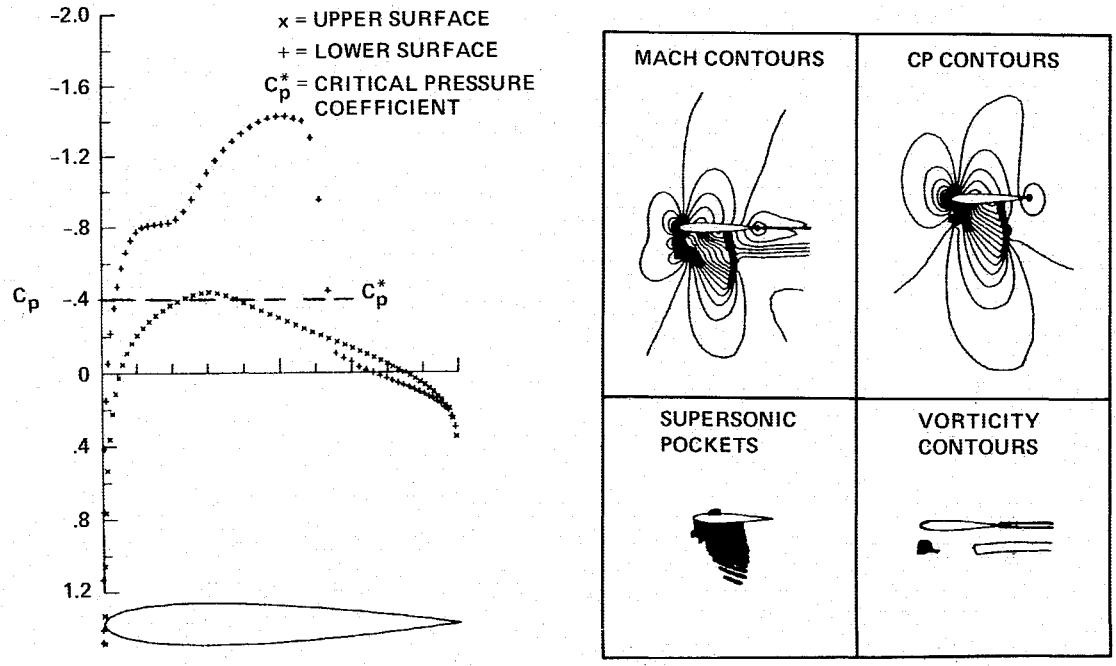

Fig. 6 Quasisteady airfoil-vortex interaction with vortex located at $x_v = 0.051c$ and $y_v = -0.26c$.

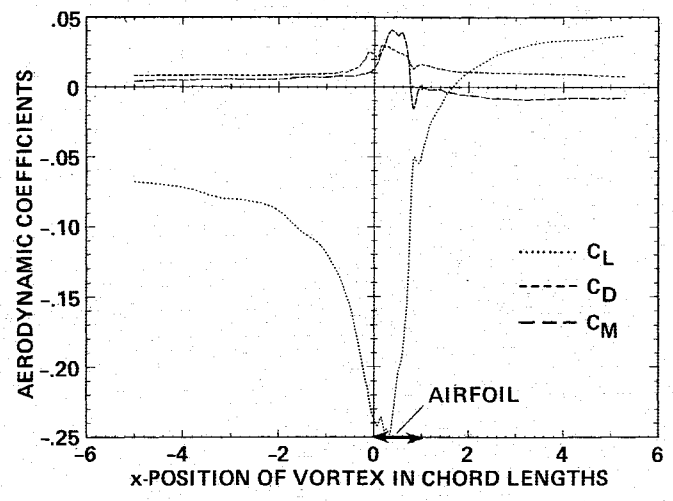

Fig. 7 Variation of aerodynamic force and moment coefficients with the instantaneous x position of the vortex during free airfoil-vortex interaction.

interaction is very strong as can be seen by the presence of a very strong shock wave on the lower surface. In such cases, the boundary layer would separate invalidating the Euler solution for this case. Similar observations are reported in Srinivasan et al.[8] This comparison shows how unsteadiness greatly moderates the influence of the vortex on the flowfield around the airfoil.

D. Unsteady Free Interaction

Finally, a free airfoil-vortex interaction in which the vortex is free to convect at local velocities is considered. The calculation of Sec. III.B. is repeated, but the vortex is made to convect at local velocities. The position of the vortex is tracked using Eq. (14). Figure 7 shows the variation of the aerodynamic force and moment coefficients with the instantaneous x position of the vortex. Comparing this with Fig. 3a, it seems that there is essentially negligible differences between the two cases except when the vortex is in the vicinity of the trailing edge of the airfoil. This is consistent with similar observations reported in Srinivasan et al.[8] In view of this, airfoil-vortex interaction can be studied by assuming that the vortex convects with the freestream velocity as long as the vortex is not too near the airfoil.

IV. Conclusions

The feasibility of using an explicit finite-volume Runge-Kutta time-stepping numerical algorithm to solve the unsteady Euler equations for the problem of inviscid transonic airfoil-vortex interaction has been demonstrated. The calculations show a significant influence of the vortex on the shock location and its strength. The strength of the interaction is much reduced in the case when the vortex is convecting past the airfoil than when it is fixed, thereby emphasizing the significant effect of unsteadiness. The calculations demonstrate the beneficial effects of the velocity-decomposition approach, and the results are in good agreement with other computations.

Acknowledgments

This research has been supported by the NASA Ames Research Center under Grant NAG 2-218. The calculations reported here were performed at the Cornell National Supercomputer Facility, which is funded, in part, by the National Science Foundation, New York State, and the IBM Corporation. The authors are grateful to Professor A. Jameson for providing the original FLO53 upon which the current investigation was based.

References

[1]Huang, M. K. and Chow, C. Y., "Trapping of a Free Vortex by Joukowski Airfoils," *AIAA Journal*, Vol. 20, March 1982, pp. 292–298.

[2]McCroskey, W. J. and Goorjian, P. M., "Interactions of Airfoils with Gusts and Concentrated Vortices in Unsteady Transonic Flow," AIAA Paper 83-1691, July 1983.

[3]Ballhaus, W. F. and Goorjian, P. M., "Implicit Finite-Difference Computations of Unsteady Transonic Flows about Airfoils," *AIAA Journal*, Vol. 15, Dec. 1977, pp. 1728–1735.

[4]Caradonna, F. X., Tung, C., and Desopper, A., "Finite-Difference Modeling of Rotor Flows Including Wake Effects," *Journal of the American Helicopter Society*, Vol. 29, No. 2, April, 1984 pp. 26–33.

[5]George, A. R. and Chang, S. B., "Flowfield and Acoustics of Two-Dimensional Blade-Vortex Interactions," AIAA Paper 84-2309, Oct. 1984.

[6]Jones, H. E., "The Aerodynamic Interaction Between an Airfoil and a Vortex in Transonic Flow," Workshop on Blade-Vortex Interactions, NASA Ames Research Center, Moffett Field, CA, Oct. 1984.

[7]Steger, J. L. and Kutler, P., "Implicit Finite-Difference Procedures for the Computation of Vortex Wakes," *AIAA Journal*, Vol. 15, April 1977, pp. 581–590.

[8]Srinivasan, G. R., McCroskey, W. J., and Kutler, P., "Numerical Simulation of the Interaction of a Vortex with a Stationary Airfoil in Transonic Flow," AIAA Paper 84-0254, Jan. 1984.

[9]Srinivasan, G. R., McCroskey, W. J., and Baeder, J. D., "Aerodynamics of Two-Dimensional Blade-Vortex Interaction," *AIAA Journal*, Vol. 24, Oct. 1986, pp. 1569–1576.

[10]Buning, P. G. and Steger, J. L., "Solution of the Two-Dimensional Euler Equations with Generalized Coordinate Transformation Using Flux Vector Splitting," AIAA Paper 82-0971, June 1982.

[11]Sankar, L. N. and Tang, W., "Numerical Solution of Unsteady Viscous Flow Past Rotor Sections," AIAA Paper 85-0129, Jan. 1985.

[12]Wu, J. C., Hsu, T. M., and Sankar, L. N., "Viscous Flow Results for the Vortex-Airfoil Interaction Problem," AIAA Paper 85-4053, Oct. 1985.

[13]Beam, R. M. and Warming, R. F., "An Implicit Finite-Difference Algorithm for Hyperbolic Systems in Conservation-law Form," *Journal of Computational Physics*, Vol. 22, Sept. 1976, pp. 87–110.

[14]Rai, M. M., "Navier-Stokes Simulations of Blade-Vortex Interaction Using High-Order Accurate Upwind Schemes," AIAA Paper 87-0543, Jan. 1987.

[15]Jameson, A., Schmidt, W., and Turkel, E., "Numerical Solutions of the Euler Equations by Finite-Volume Methods Using Runge-Kutta Time-Stepping Schemes," AIAA Paper 81-1259, June 1981.

[16]Turkel, E., "Acceleration to a Steady State for the Euler Equations," Institute for Computer Applications in Science and Engineering, Hampton, VA, ICASE Rept. 84-32, NASA CR-172398, July 1984.

[17]Jameson, A. and Baker, T. J., "Multi-Grid Solutions of Euler Equations for Aircraft Configurations," AIAA Paper 84-0093, Jan. 1984.

[18]Damodaran, M., "Numerical Calculation of Unsteady Inviscid Rotational Transonic Flow Past Airfoils Using Euler Equations," Ph.D. Thesis, Cornell Univ. Ithaca, NY, Jan. 1987.

[19]McCroskey, W. J. and Srinivasan, G. R., Workshop on Blade-Vortex Interactions, NASA-Ames Research Center, Moffett Field, CA, Oct. 1984.

[20]Srinivasan, G. R., private communication, Feb. 1987.